sustainability

MDPI

Article

Study on the Effect of Non-Linear Ventilation Pipe Composite Measures on the Slope Permafrost Subgrade

Zhe Cheng, Zhilong Zhang *, Guang Liu and Ying Wu

School of Civil Engineering and Architecture, Xinjiang University, Urumqi 830049, China
* Correspondence: zhangzl@xju.edu.cn

Abstract: In the alpine mountain area, the stability of the steep-slope permafrost subgrade is mainly affected by the temperature variation in the frozen soil layer at the base of the road. Under the conditions of climate warming and engineering-related disturbance, the cooling of the subgrade is an urgent problem to be solved in the field of construction. In this paper, the numerical calculation method, combined with data monitored in situ, is used to study the cooling effects of several subgrade cooling measures, in which the non-linear ventilation pipe and rubble layer are combined. The results show the following: (1) the temperature field of the steep-slope subgrade is clearly different in lateral terms—after 20 years of operation, the maximum difference in the melting depth between the left shoulder and the subgrade center is 3 m; (2) the maximum melting depth of the gravel subgrade center is 3.85 m, while the maximum difference in the melting depth between the left shoulder and the subgrade center is 2.3 m; (3) the cooling effect of the composite measures is noteworthy, and a −2.2 °C freezing area appears under the subgrade.

Keywords: steep-slope permafrost; half-cut and half-fill subgrade; non-linear vent pipe gravel layer; cooling effect

check for updates

Citation: Cheng, Z.; Zhang, Z.; Liu, G.; Wu, Y. Study on the Effect of Non-Linear Ventilation Pipe Composite Measures on the Slope Permafrost Subgrade. *Sustainability* **2023**, *15*, 1180. https://doi.org/10.3390/su15021180

Academic Editors: Pengjiao Jia, Peixin Shi, Cheng Cheng and Xi Jiang

Received: 28 October 2022
Revised: 26 December 2022
Accepted: 29 December 2022
Published: 9 January 2023

1. Introduction

During the "Fourteenth Five Years Plan" period, Xinjiang accelerated the construction of a transportation hub in the core area of the Silk Road Economic Belt, where the Kunlun Mountains, Tianshan Mountains and Altai Mountains are distributed. The annual average temperature is lower than −3 °C, which creates permafrost and segregated areas where the frozen ground is widely distributed [1,2] Therefore, the construction project has many technical difficulties due to the harsh climate, such as the cold temperature, high altitude and high latitude. Slope road engineering can lead to the disturbance of natural frozen soil [3], resulting in dramatic changes in the original soil temperature. Disturbances such as uneven settlement, longitudinal cracks and road boiling occur frequently, and seriously threaten the safe operation of the roads.

As a measure for actively regulating the ground temperature, the crushed stone subgrade has been widely used in road engineering in permafrost regions, in which the convection and conduction modes of cold air are used to increase the cooling capacity of the subgrade and protect the permafrost under the subgrade by changing the embankment structure. Through indoor tests, Yu found that crushed and block stone layers with a certain thickness had obvious cooling effects [4–6]. Lai Yuanming studied the natural convection effect and cooling effect of block stone particles with different sizes when the top temperature fluctuated [7–9] Cheng conducted experimental analyses on the cooling effects of gravel subgrade structures with different shapes [10,11], and found that the ventilation pipe subgrade is one of the effective engineering measures employed to maintain subgrade stability in permafrost regions.

Under the impact of natural convection and wind, cold air with a high density can extrude the hot air in the pipe and constantly remove the heat from the surrounding soil to "cool the subgrade", thus reducing the ground temperature of the permafrost under the subgrade and improving the thermal stability [12]. Indoor model tests show that the vent pipe can effectively reduce the temperature at the bottom of the embankment and the maximum melting depth [9,13,14]. Relevant studies have confirmed that the diameter, laying spacing and buried height of the ventilation pipe and the ambient wind speed all have significant impacts on the cooling effect of the ventilation pipe subgrade [15–21]). According to the convection heat transfer process [11,20], it is demonstrated that the intensity of the forced convection in the pipe is greater than that of natural convection. When the heat transfer of the viscous layer and tube wall is ignored, it is found to be mainly affected by wind speed.

Currently, engineering construction mainly adopts the abovementioned measures that are combined with anti-slip piles or retaining walls and other types of mechanical support to achieve noteworthy results. However, in the case of the Xinjiang alpine mountain road project, a steeper slope of the high-temperature permafrost section was carried out due to the roadbed's half-road rift design; the fact is that there is only a single slope and the rainfall, thick winter snow and other factors, as well as the excavation of the roadbed and slope stability are seriously inadequate, and there is even a risk of slippage at the titled freeze–thaw interface. Corresponding to the above-mentioned problems, the multi-year permafrost section in the Middle Tianshan Mountains of Xinjiang was taken as an example in this paper, and we proposed a new composite-measure roadbed and employed numerical calculation methods to study the law of the hydrothermal changes in the steep-slope permafrost roadbed; the water migration and temperature change in soil under different measures were revealed, which can be used as a theoretical basis for studying frost heaving deformation of the roadbed and provide a theoretical reference for the construction of alpine mountain road projects in the future.

2. Geometric Model

According to the standard for the Design of Highway Routes [21] and the survey data of the G218 Line in the hinterland of the Central Tianshan Mountains [22–24] the physical structure of the highway subgrade and its asphalt pavement are shown in Figure 1. The width of the model at the upper and lower slope toe of the subgrade is 50 m, the depth is 30 m, and the slope angle is 25°. In order to realize the best cooling effect, it is necessary to release the heat of the asphalt pavement road and protect the permafrost layer; for this purpose, four different subgrade structures were designed in this study. The specific physical parameters of the soil layer are listed in Tables 1 and 2.

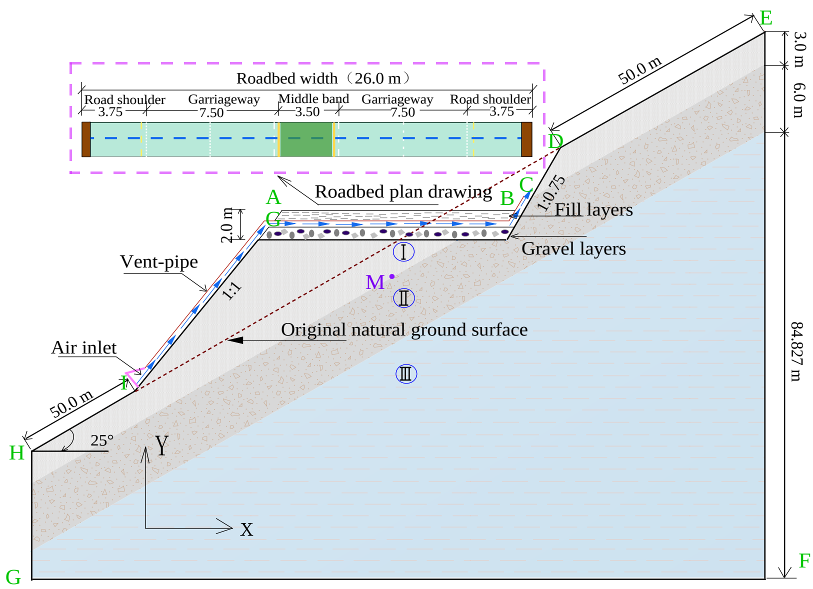

Figure 1. Subgrade Model with Composite Measures.

Table 1. Thermodynamic parameters of the soil layer [25,26].

Material	ρ_d/ $(kg \cdot m^{-3})$	λ_f/ $W \cdot (m \cdot K)^{-1}$	λ_u/ $W \cdot (m \cdot K)^{-1}$	C_f/ $kJ \cdot (m^3 \cdot K)^{-1}$	C_u/ $kJ \cdot (m^3 \cdot K)^{-1}$	Water Content/%
Fill soil	1940	1.98	1.919	1913	2227	8
Silt	1600	0.97	1.09	1932	2341	11
Gravel soil	1500	1.351	1.125	1879	2357	15
Mudrock	1800	1.824	1.474	1846	2099	10
Crushed rock	1950	0.387	0.385	1180	1180	0

Table 2. Soil moisture related parameters [27].

Material	$a/(1 \cdot m^{-1})$	m	l	θ_s	θ_r	$k_s/(m \cdot s^{-1})$
Fill soil	0.45	0.50	0.50	0.25	0.01	4×10^{-6}
Silt	2.59	0.22	0.50	0.50	0.03	1×10^{-6}
Gravel soil	2.00	0.38	0.50	0.50	0.05	5×10^{-6}
Mudrock	0.80	0.50	0.50	0.30	0.01	1×10^{-9}

Working condition 1: filling the subgrade without protection and using excavation and backfilling to form the subgrade at the natural slope. According to the relevant surveys, the natural slope soil mass is divided into three layers [23,24,28,29] from top to bottom. The first layer is silty soil with a thickness of 3 m, the second layer is crushed and block stone soil with a thickness of 6 m, and the third part is weathered mudstone with a thickness of 21 m.

Working condition 2: the gravel layer subgrade—adding a gravel layer to the subgrade after excavation. The gravel grain size is 7~13 cm, with an average value of 10 cm [30]. The gravel layer is 1.4 m in thickness, and the overburdened soil is 1.4 m in thickness.

Working condition 3: ventilation pipe subgrade—a concrete ventilation pipe is installed on the subgrade after excavation. The diameter of the ventilation pipe is 0.4 m, the wall thickness is 0.05 m, and the thickness of the backfill on the vent pipe is 1.5 m.

Working condition 4: the gravel layer composite subgrade with a non-linear ventilation pipe is covered by a gravel layer with a thickness of 1 m after excavation and average particle size of 10 cm. The ventilation pipe, with a diameter of 0.4 m and a wall thickness of 0.05 m, is installed above the gravel layer, and the filling soil over the ventilation pipe is 0.5 m thick.

3. Mathematical Model and Boundary Conditions

3.1. Flow Equation

The water in the soil will migrate with the soil temperature changing, and the migration process is assumed to follow Darcy's law [27,31–33]. According to Richard's equation, the control equation of water separation field used in this paper is:

$$\frac{\partial \theta_u}{\partial t} + \frac{\rho_i}{\rho_w} \cdot \frac{\partial \theta_i}{\partial t} = \nabla [D(\theta_u) \nabla \theta_u + k_g(\theta_u)] \tag{1}$$

where θ_u is the volume of unfrozen water; k_g is the permeability coefficient of the unsaturated soil in the direction of gravity acceleration and $D(\theta_u)$ is the water diffusion rate in the frozen soil. The calculation formula is:

$$D(\theta_u) = \frac{k(\theta_u)}{c(\theta_u)} \cdot I \tag{2}$$

where $k(\theta_u)$ is the soil permeability (m/s); $c(\theta_u)$ is the specific water capacity $(1/m)$ and I is the impedance factor ($I = 10^{-10\theta_i}$). The connection equation is:

$$B_i = \frac{\theta_i}{\theta_u} = \begin{cases} 1.1(\frac{T}{T_f})^B - 1 & (T < T_f) \\ 0 & (T \geq T_f) \end{cases} \tag{3}$$

where B is a constant and is related to the soil type and salt content; according to the empirical data, its value can respectively be taken as 0.61 for sand, 0.56 for clay and 0.47 for silt.

3.2. Heat Transfer Equation

In soil heat transfer, the effects of convection and mass transfer are ignored, while only heat conduction and phase change are considered [34]. The differential equation for soil heat conduction is:

$$\rho C(\theta)\frac{\partial T}{\partial t} = \nabla \cdot (\lambda(\theta)\nabla T) + L \cdot \rho_i \frac{\partial \theta_i}{\partial t} \tag{4}$$

where T is the instantaneous temperature of the soil mass (°C); t is the time (s); ρ and ρ_i are the density of soil and ice (kg/m^3); L is the latent heat of the phase change; θ is the volume of the water content ($\theta = \theta_u + \rho_i/\rho_w \cdot \theta_i$); θ_i is the volume of the ice content; $C(\theta)$ is the volumetric heat capacity of the soil $(J/(kg \cdot K))$; $\lambda(\theta)$ is the heat conduction of the soil $(W/(m \cdot K))$ and $(T_f - \Delta T, T_f + \Delta T)$ is the temperature range of the ice–water phase transition.

$$C(\theta) = \begin{cases} C_f & T < T_f - \Delta T \\ \frac{L}{2\Delta T} + \frac{C_f + C_u}{2} & T_f - \Delta T \leq T \leq T_f + \Delta T \\ C_u & T > T_f + \Delta T \end{cases} \tag{5}$$

$$\lambda(\theta) = \begin{cases} \lambda_f & T < T_f - \Delta T \\ \lambda_f + \frac{\lambda_u - \lambda_f}{2\Delta T}\left[T - \left(T_f - \Delta T\right)\right] & T_f - \Delta T \leq T \leq T_f + \Delta T \\ \lambda_u & T > T_f + \Delta T \end{cases} \tag{6}$$

3.3. Air Flow Control Equation of the Ventilation Pipe

In general, the critical Reynolds number for maintaining the laminar flow in the pipe is $R_e = 2300$. Referring to the relevant research on the Qinghai Tibet Plateau [35–37], under the 0 °C condition, the motion viscosity coefficient of the air is $u = (2.3 \sim 2.73) \times 10^{-5}\ \mathrm{m^2/s}$. For a ventilation pipe with an inner diameter of 0.4 m, its critical velocity is:

$$V_{ij} = \frac{uR_e}{d} = 0.132\ \mathrm{m/s} \tag{7}$$

According to the calculation results, in the ventilation pipe, the deconstructed laminar and turbulent critical velocity is very low, making it almost impossible for the air to flow in the laminar form. Thus, the air heat exchange of the forced convection in the ventilation pipe is turbulent, so the model $k - \varepsilon$, with good applicability, is selected:

$$\frac{\partial}{\partial t}(\rho k) + \frac{\partial}{\partial x_i}(\rho k u_i) = \frac{\partial}{\partial x_j}\left[\left(\mu + \frac{\mu_t}{\sigma_k}\right)\frac{\partial k}{\partial x_j}\right] + G_k + G_b - \rho\varepsilon - Y_M + S_k \tag{8}$$

$$\frac{\partial}{\partial t}(\rho \varepsilon) + \frac{\partial}{\partial x_i}(\rho \varepsilon u_i) = \frac{\partial}{\partial x_j}\left[\left(\mu + \frac{\mu_t}{\sigma_\varepsilon}\right)\frac{\partial \varepsilon}{\partial x_j}\right] + G_{1\varepsilon}\frac{\varepsilon}{k}(G_k + G_{3\varepsilon}G_B) - G_{2\varepsilon}\rho\frac{\varepsilon^2}{k} + S_\varepsilon \tag{9}$$

where ρ is the air density; k is the pulsating kinetic energy; ε is the pulsating kinetic energy dissipation rate; t is time; u_i is the velocity component of the air in the direction i; x_j is the displacement of the air in the direction j; σ_k and σ_ε are, respectively, the Prandtl number corresponding to the turbulence kinetic energy k and dissipation rate ε; G_k is the turbulence kinetic energy generated by the laminar velocity gradient; G_b is the turbulence kinetic energy generated by buoyancy; Y_M is the contribution of the fluctuation expansion of compressible turbulence to the total dissipation rate; S_k and S_ε are user-defined source terms; $G_{1\varepsilon}$, $G_{2\varepsilon}$ and $G_{3\varepsilon}$ are empirical constants; μ is the aerodynamic viscosity and μ_t is the turbulent viscosity coefficient of the air (Table 3).

Table 3. Air-related physical parameters [38].

Physical Parameters	$\rho_a/(\mathrm{kg \cdot m^{-3}})$	$C_a/\mathrm{kJ \cdot (m^{-3} \cdot K)^{-1}}$	$\lambda_a/\mathrm{W \cdot (m \cdot K)^{-1}}$	$\mu/(\mathrm{P_a \cdot s})$
Air	0.641	1004	0.025	1.75×10^{-5}

3.4. Control Equation of Natural Air Convection in the Gravel Layer

The gravel layer can be regarded as a porous medium with high permeability, in which the internal natural convection is unsteady, with a non-isothermal flow. Its control equations include the continuity equation, momentum equation and energy equation [39–42], as follows:

Continuity equation:

$$\frac{\partial v_x}{\partial x} + \frac{\partial v_y}{\partial y} = 0 \tag{10}$$

where v_x and v_y are, respectively, the velocity of the air in the gravel layer in the direction x, y.

Momentum equation:

$$\begin{array}{c} \frac{\partial p}{\partial x} = -\frac{u}{k} v_x - \rho_a B|v|v_x \\ \frac{\partial p}{\partial y} = -\frac{u}{k} v_y - \rho_a B|v|v_y - \rho_a^* g \end{array} \tag{11}$$

In general, the critical Reynolds equation for maintaining laminar flow in the pipe is as follows: v is the velocity, with $|v| = \sqrt{v_x^2 + v_y^2}$ for reference; ρ_a is the air density; p is the air pressure; u is the aerodynamic viscosity coefficient; k is the air permeability coefficient, with $k = \frac{d_p^2 \cdot \varepsilon_p^3}{180(1-\varepsilon_p)^2}$ and B is the inertial resistance coefficient (not the Beta factor of the Darcy flow), so $B = \frac{1.75(1-\varepsilon_p)}{d_p \varepsilon_p^3}$. Using Boussinesq to fit the relationship between the air density and temperature, $\rho_a^* = \rho_{a0}[1 - \beta(T - T_0)]$, β is the coefficient of the thermal expansion of the air and T and T_0 are the temperature and the reference value.

Energy equation:

$$C(\theta)^* \frac{\partial T}{\partial t} = \lambda(\theta)^* \left(\frac{\partial^2 T}{\partial x^2} + \frac{\partial^2 T}{\partial y^2} \right) + C_a \left(v_x \frac{\partial T}{\partial t} + v_y \frac{\partial T}{\partial y} \right) \tag{12}$$

where $C(\theta)^*$ is the equivalent volumetric heat capacity of the gravel layer, $\lambda(\theta)^*$ is the equivalent thermal conductivity of the gravel layer and C_a is the volume heat capacity of the air.

3.5. Boundary Conditions and Model Parameters

Considering the area where the project is located, along the Naba Road in the permafrost region (Alagou Township, Bazhou and Jingxian County, Xinjiang), with an altitude of 3270 m, the observation data from the meteorological stations are selected. According to the boundary layer effect [43] the temperature is simplified into a trigonometric function considering the effect of global warming [44]) (the temperature has increased by 2.6 °C in the last 50 years). The temperature fitting results are shown in Figure 2. Referring to the fitting results of the asphalt pavement temperature and slope surface temperature and the measured data of the Qinghai Tibet Highway [45], the function of the final temperature is obtained.

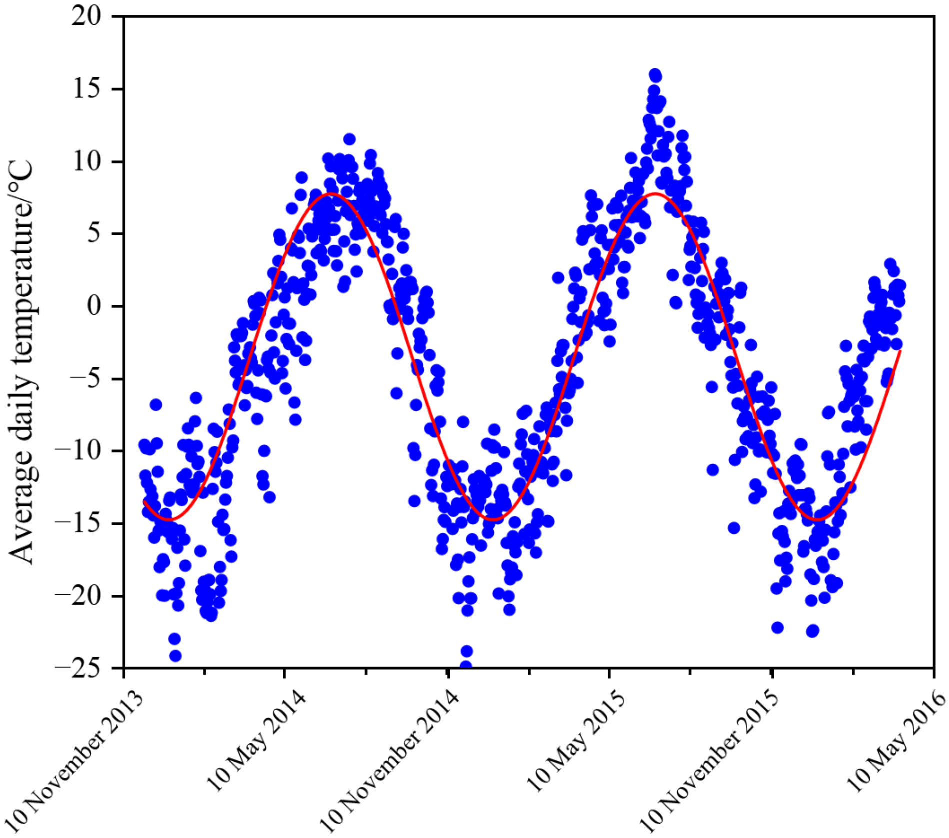

Figure 2. Atmospheric Temperature Change in Baluntai Town.

Baluntai Town is located in the hinterland of the Tianshan Mountains and is high in the north and low in the south; it has a typical continental climate, which is hot and dry in the summer, with the highest annual temperature of 18 °C in the middle of July. The winter there is cold with a bit of snow, and the lowest temperature is −25 °C around January. The specific fitting functions are as follows:

Atmospheric temperature:

$$T = -3.5 + 11.25 \sin\left(\frac{2\pi}{8760} t_h + \frac{\pi}{2} - \frac{1}{2}\right) + \frac{2.6}{8760} t_h \tag{13}$$

Natural ground temperature:

$$T = -1.5 + 12 \sin\left(\frac{2\pi}{8760} t_h + \frac{\pi}{2} - \frac{1}{2}\right) + \frac{2.6}{8760} t_h \tag{14}$$

The temperature of the subgrade's external slope surface:

$$T = -0.5 + 13 \sin\left(\frac{2\pi}{8760} t_h + \frac{\pi}{2} - \frac{1}{2}\right) + \frac{2.6}{8760} t_h \tag{15}$$

Subgrade surface temperature:

$$T = 2.5 + 14 \sin\left(\frac{2\pi}{8760} t_h + \frac{\pi}{2} - \frac{1}{2}\right) + \frac{2.6}{8760} t_h \tag{16}$$

The boundary conditions on both sides of the subgrade are adiabatic, and the boundary conditions at the bottom of the subgrade are heat flux: $q = 0.06$ (W/m^2).

The ambient wind speed is the main factor affecting the cooling effect of the ventilation pipe. According to the long-term monitoring data of Balun meteorological station, it is known that the local annual average wind speed is 3.4 m/s, and the wind speed is relatively high from June to July and December to January, with the highest value of 17 m/s (Figure 3). According to the relationship between the wind speed at the base of the ventilation pipe and the ambient wind speed in the Beilu River of the Qinghai Tibet Plateau [46], the average wind speed at the inlet of the ventilation pipe is 1 m/s.

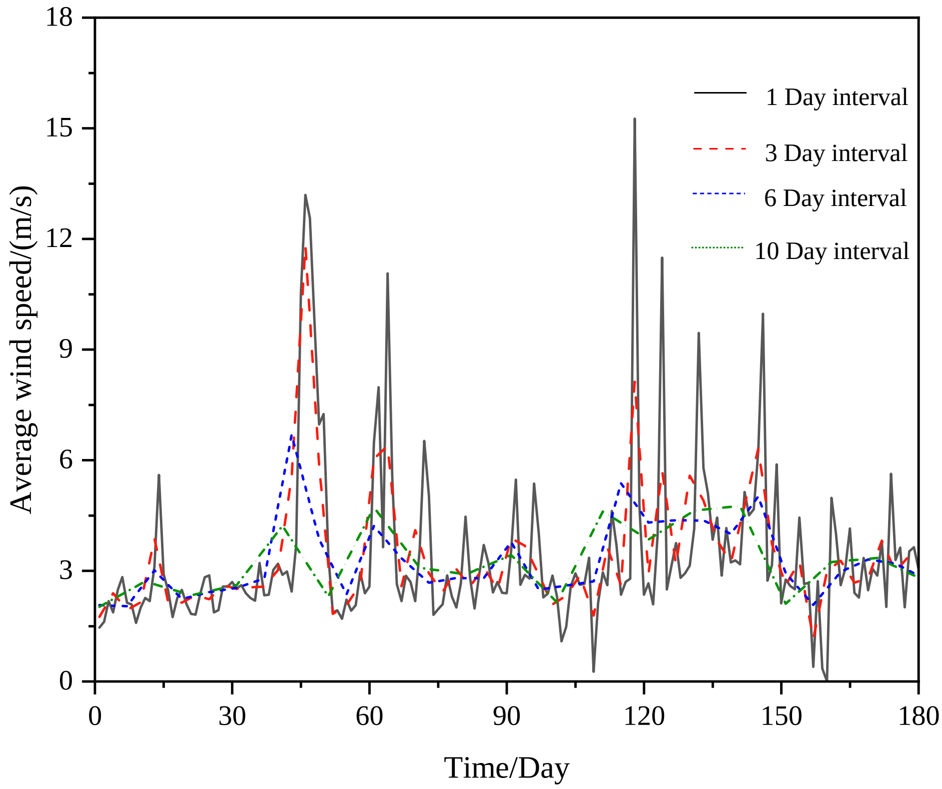

Figure 3. Curve of the Average Wind Speed at Different Time Distances in Baluntai Town.

4. Results and Analysis

4.1. Model Verification

In order to verify the rationality of the simulation and the accuracy of the calculation results, the actual recorded temperature of the natural slope ground is compared with the simulation results.

The elevation of the K600 + 000~K474~690 section of the project is between 3040~3230 m. The permafrost in this section is relatively developed. With geological radar detection, it is preliminarily determined that the upper limit of permafrost in this area is between 2.3 m and 3.4 m. The calculation results show that the upper limit of permafrost in this area is 3 m. It can be seen from Figure 4 that the calculated results are in substantial agreement with the measured values, and the overall change trend is basically the same. When the measurement depth is less than 2.5 m, the ground temperature is greater than 0 °C. When the measurement depth is 2.5~3.5 m, the ground temperature is between −0.5 and 0.5 °C. When the measurement depth is more than 3.5 m, the ground temperature is between −0.5 and −1 °C, and the temperature change is moderate, indicating that the calculation results can better reflect the actual situation of the change in the subgrade temperature.

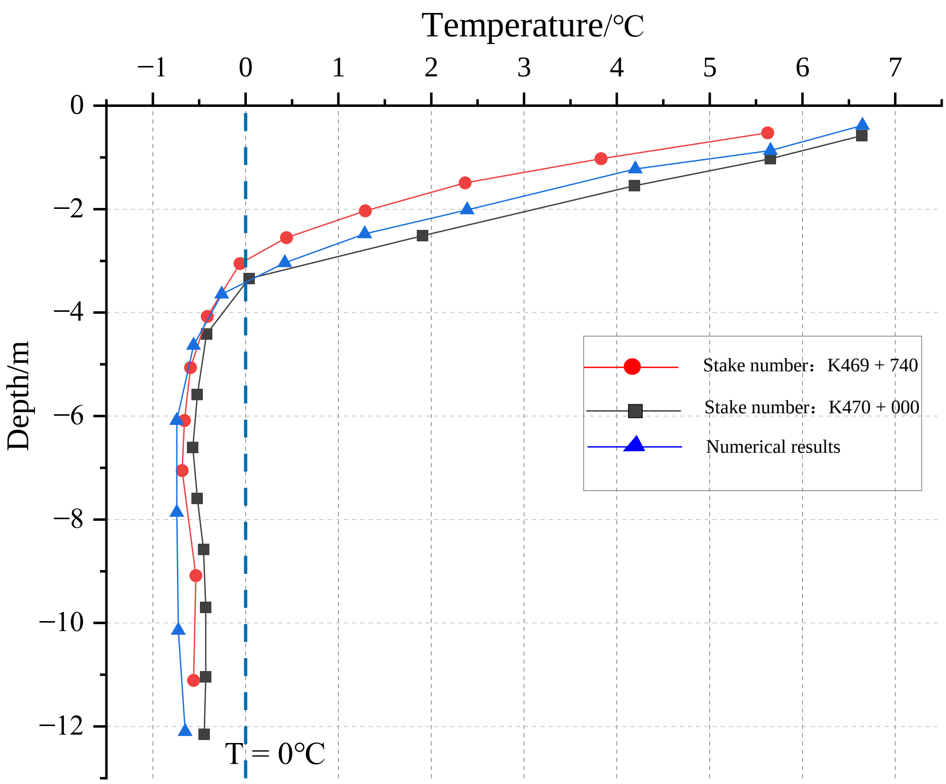

Figure 4. Comparison of the Measured Ground Temperature and Simulated Ground Temperature of the Natural Slope Surface of the Subgrade.

4.2. Analysis of the Subgrade Temperature State

In order to evaluate the cooling performance of the composite subgrade, the temperature of four different subgrade structures over 20 years were simulated. The maximum melting depth of the frozen soil subgrade in the alpine mountain area is usually reached in October. The temperature disatribution of the subgrade on 15 October in the 10th and 20th year is analyzed in this paper.

In mid-July, with the increase in atmospheric temperature and solar radiation, the upper boundary temperature reached the highest value of 16 °C in a year, and the temperature of the soil below the subgrade was lower than 0 °C. As the upper heat was transferred downward, the whole roadbed turned into an endothermic state. In mid-October, with the decrease in temperature, the slope on both sides of the subgrade first appeared negative temperature, while the inside soil accumulated a lot of heat and diffused around. As shown in Figure 5, in the middle of October in the 10th year, the maximum thawing depth of the wide pavement was 8 m, which is 5 m deeper than the maximum thawing depth of the natural slope of 3 m, indicating that the downward heat transfer at the top of the subgrade has a certain lag. With the accumulation of heat, this phenomenon became more significant in the 20th year, with a maximum melting depth of 12 m. It can be seen from the change in the −0.35 °C isotherm that the deep permafrost is also deteriorating, and the degradation of the permafrost and the melting of the upper soil layer change the mechanical properties of the soil, which results in the settlement of the subgrade and is not conducive to the stability of the subgrade.

Due to the convective heat transfer process, the crushed stone subgrade can cool the frozen soil subgrade. As shown in Figure 6, at the center of the gravel subgrade, the maximum melting depth in the 10th year was 3.85 m, which is almost the same as that in the 20th year. Compared with the ordinary subgrade, the upper limit of the frozen soil obviously rose, but the temperature of the permafrost layer under the subgrade was relatively high; the frozen soil layer was still in a degraded state, with the −0.35 °C isotherm dropping from 5.5 m in the 10th year to 7.5 m in the 20th year. Therefore, crushed stone subgrade technology cannot effectively solve the problem of the intense heat absorption of the asphalt pavement.

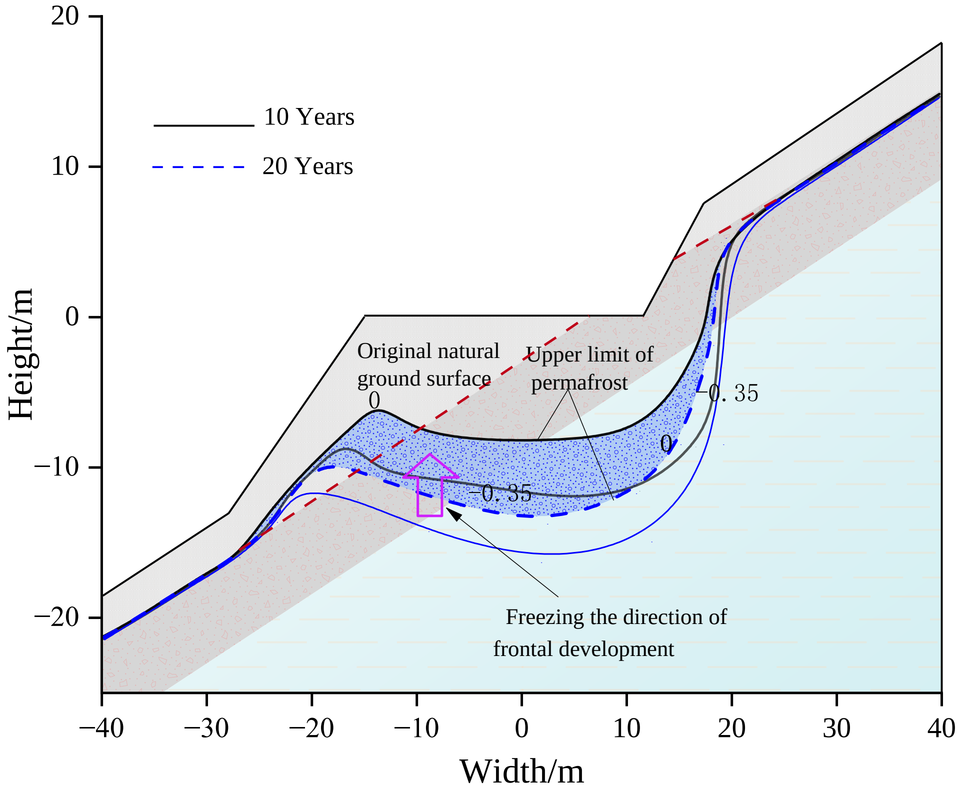

Figure 5. Temperature Distribution of the Ordinary Subgrade on 15 October in the 10th and 20th Years.

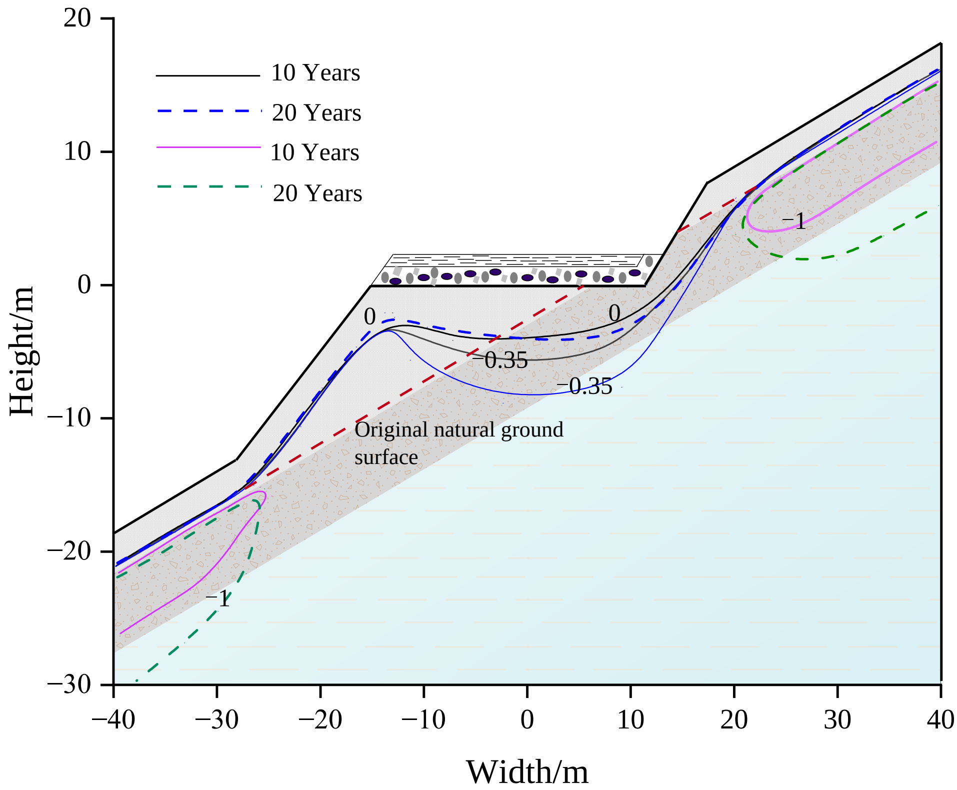

Figure 6. Temperature Distribution of the Crushed Stone Subgrade on 15 October in the 10th and 20th Years.

Figure 7 shows the temperature distribution of the ordinary ventilation pipe subgrade on the 15th day of October in the 10th and 20th operation years. The average annual temperature of the area where the Naba Road is located is −3.5 °C, and the average annual wind speed is 3.4 m/s. It can be seen from Figure 7 that the 0 °C isotherm is smooth, and the maximum melting depth under the pavement is 1.45 m, which is 6.55 m higher than that of the ordinary subgrade. The melting depth in the 10th year is basically the same as that in the 20th year; however, the melting depth of the frozen soil on both sides of the ventilation pipe subgrade is significantly increased, as well as the air inlet and air outlet sections while the −0.35 °C isotherm continues to develop in downward trend from the 10th year to the 20th year. Thus, the conventional ventilation pipe subgrade cannot reduce the temperature of the wide pavement subgrade.

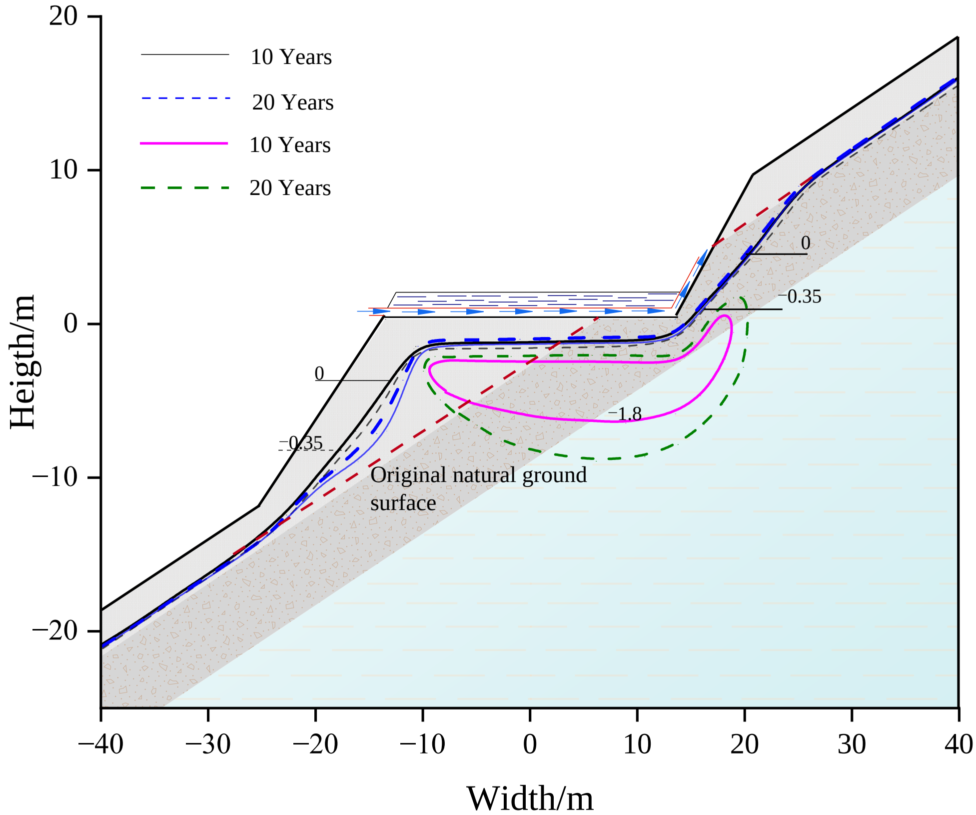

Figure 7. Temperature Distribution of the Ventilation Duct Subgrade on 15 October in the 10th and 20th Years.

In the cold season, the heat exchange between the warm stratum and cold environment can be intensified through composite measures. As shown in Figure 8, in the 10th year, the temperature of the deep-frozen soil layer of the subgrade is decreased significantly, and a −2.2 °C isotherm appears at 4 m below the pavement and forms a frozen area. In the 20th year, the frozen area is more clearly developed in the lateral and slope directions of the subgrade. From the 10th to 20th years, the 0 °C isotherm and −0.35 °C isotherm change little and are distributed smoothly and evenly in the transverse and slope directions of the subgrade. The lateral cooling area is deep, which can effectively reduce the risk of uneven settlement of the subgrade.

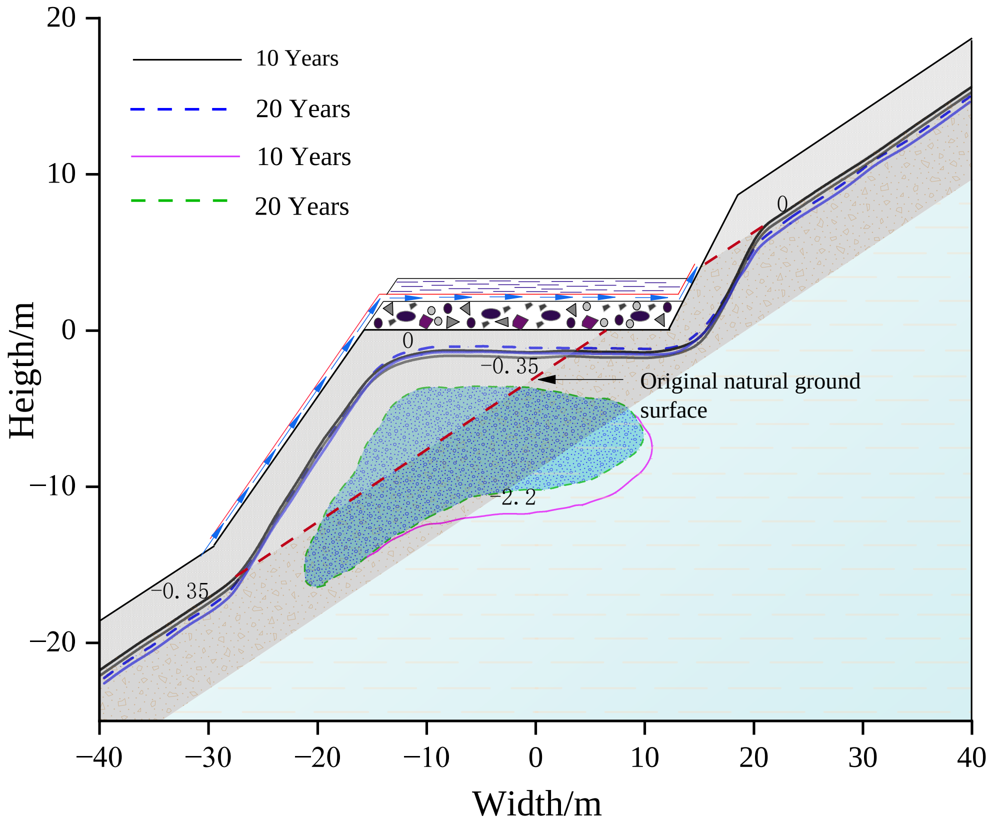

Figure 8. Temperature Distribution of the Composite Subgrade on 15 October in the 10th and 20th Years.

4.3. Analysis of the Temperature Change Process

It can be seen from Figure 9 that the temperature of the ordinary subgrade is the highest, especially at a depth of 2~−8 m, and the highest temperature is 6 °C. The cooling effect of the gravel subgrade is poor, and the temperature above 0 m is higher than that of the ordinary subgrade, which is due to the natural convection effect of the gravel layer in the cold season. At a depth of −4 m, the temperature is 1 °C, which is 2 °C lower than that of the ordinary subgrade. At the center of the subgrade, both the ventilation pipe subgrade and the composite subgrade can effectively cool the subgrade. The temperature of the composite subgrade is approximately −2 °C at a depth of −4 m~−12 m, and the temperature of the permafrost layer is approximately −1.5 °C below the depth of −12 m, indicating better thermal stability.

The change in the instantaneous heat flux at the bottom of the subgrade after 20 years is shown in Figure 10. It can be seen that heat absorption mainly occurs in the warm seasons, and heat dissipation mainly occurs in the cold seasons. The heat absorption of the ordinary subgrade lasts from the end of March to the end of September, and the maximum heat flux can reach 6.9 W/m^2, which occurs from June to the middle of July. The gravel subgrade's heat absorption and release process are similar to those of the ordinary subgrade, with a maximum heat absorption flux of 4.2 W/m^2 in the middle of July and a maximum heat release of −5 W/m^2 in the middle of December. The changes in the heat flux at the base of the ventilation pipe subgrade and the composite road are similar. The maximum heat absorption of the ventilation pipe subgrade is 3 W/m^2 in the middle of July, and the maximum heat release is −3.5 W/m^2 in the middle of December. The maximum heat absorption of the composite subgrade is 2.1 W/m^2, and the maximum heat release is −2.15 W/m^2. The overall heat absorption and release are basically the same, and the process is mild, indicating that the thermal stability of the subgrade is acceptable.

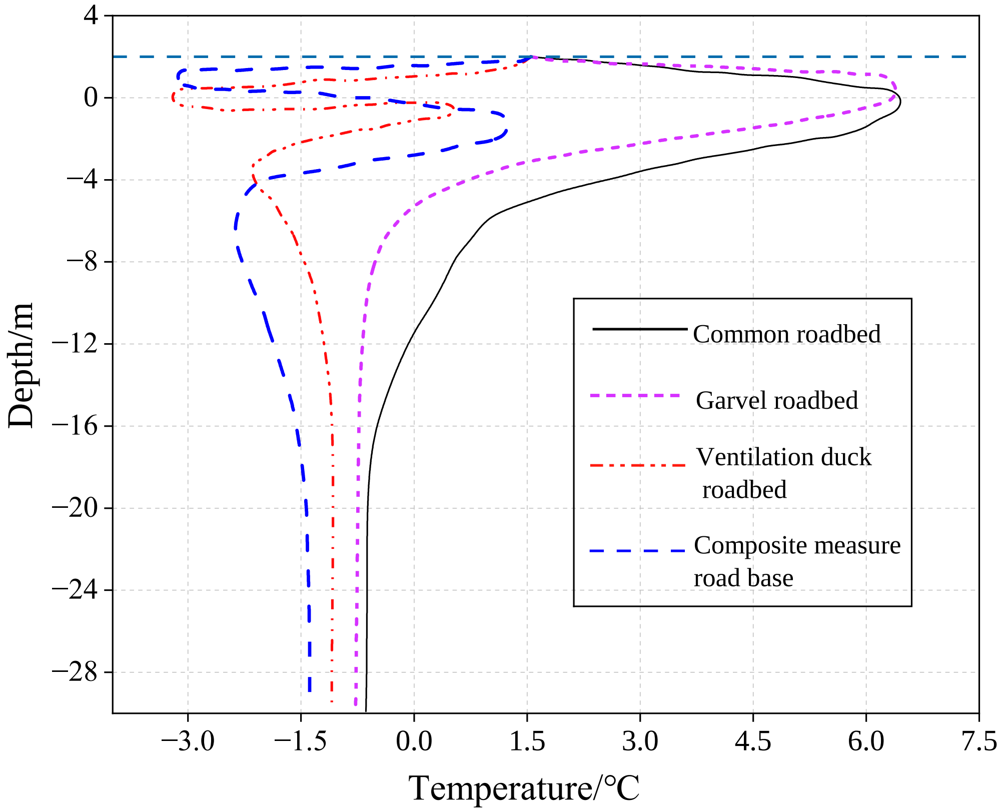

Figure 9. Temperature Change of the Subgrade Centerline with Depth on 15 October, 20th Year.

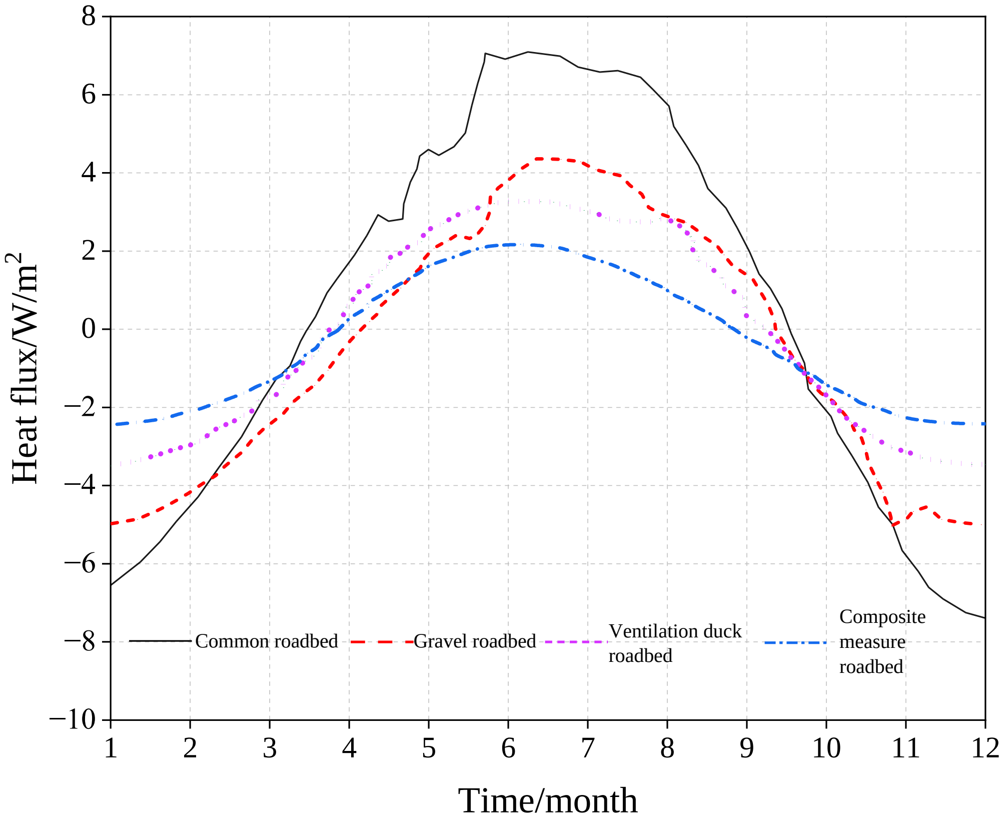

Figure 10. Change in the heat flux of the road base in the 20th year.

Figure 11a shows the trend of the maximum melting depth at the center of the different subgrades, and it can be observed that their maximum melting depth varies greatly. The maximum melting depth of the ordinary subgrade increases over time. The melting rate is approximately 0.5 m/a, and there is no stable trend. The melting rate of the block stone subgrade is basically the same as that of the ordinary subgrade in the first 8 years, and the change rate is relatively low. The maximum melting depths of the composite subgrade and ventilation pipe subgrade show a rising trend and tend to be stable after the 15th year. Figure 11b shows the temperature trend at the midpoint of the composite roadbed at a 10 m depth, with year 5 as the starting time; it can be seen that there is essentially no change in the −2 °C freeze zone after 12 years, suggesting that the influences of half-cut, half-fill and climate warming on the subgrade can be ignored.

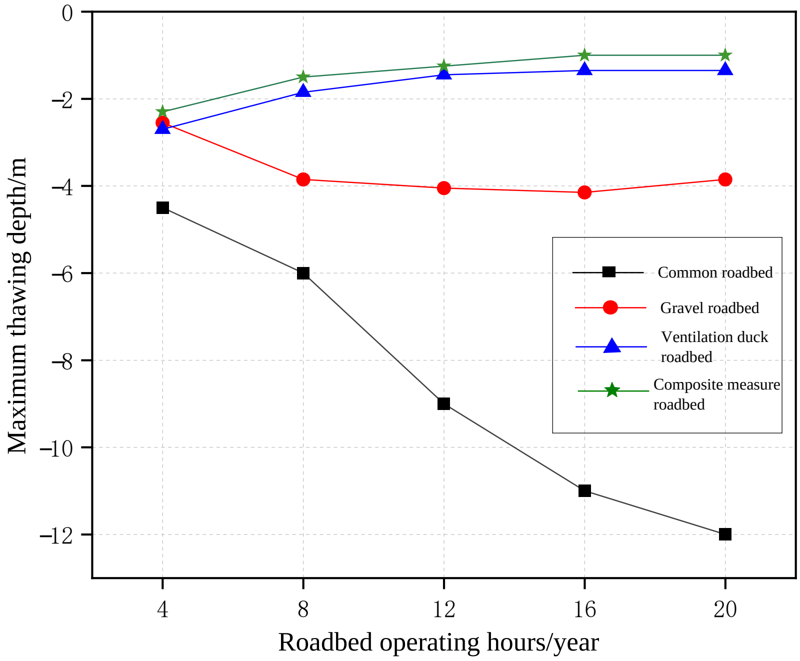

(**a**)

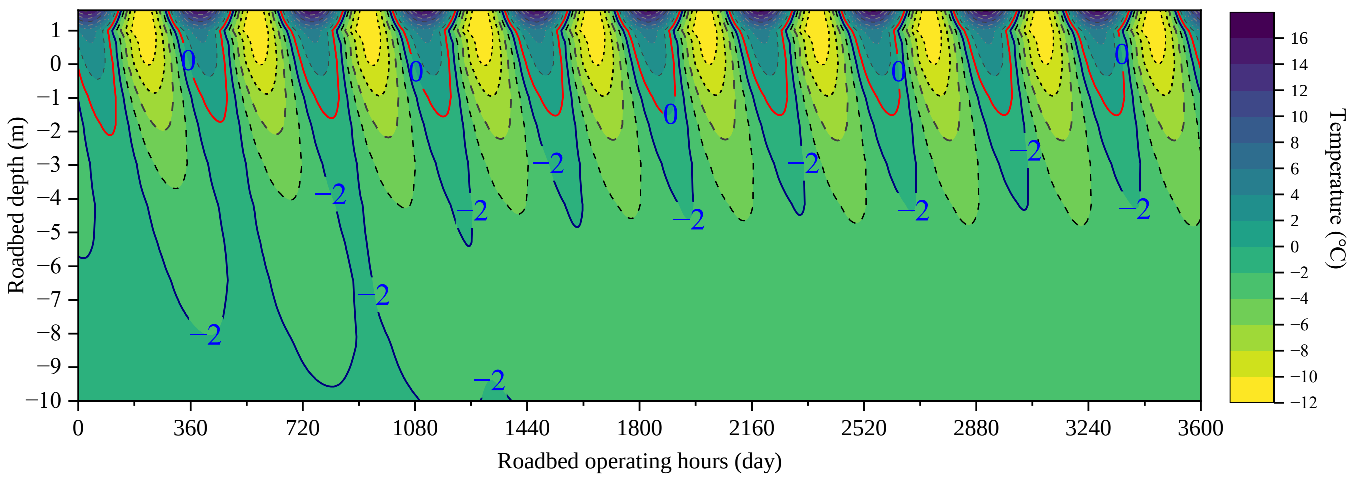

(**b**)

Figure 11. The variation in the maximum melting depth of the subgrade. (**a**) Variation of maximum thawing depth with time at subgrade center, (**b**) Variation of temperature at the center of composite subgrade with time.

Firstly, after the embankment's construction, the temperature at point M (3 m below the original natural slope) decreases with the decrease in temperature and then changes periodically within the next 20 years, as shown in Figure 12. In the case of the ordinary subgrade and crushed stone subgrade, both their temperatures increase. At point M, although the temperature of the ordinary subgrade and crushed stone subgrade is higher than the freezing temperature of the stratum (0 °C), the temperature of the crushed stone subgrade is significantly lower than that of the ordinary subgrade, and their maximum temperature difference can reach 2.3 °C. In addition, at point M, the temperature changing trends of the ventilation duct subgrade and composite subgrade are also very similar, and they both decrease to a negative value after the 10th year. However, due to the comprehensive cooling effect of the composite subgrade, the temperature of the composite subgrade is lower than that of the ventilation pipe subgrade, and the maximum temperature difference is 0.6 °C. In general, the annual cycle of the temperature change of composite subgrade is small, and the temperature of the permafrost is low, indicating that the overall cooling effect is good.

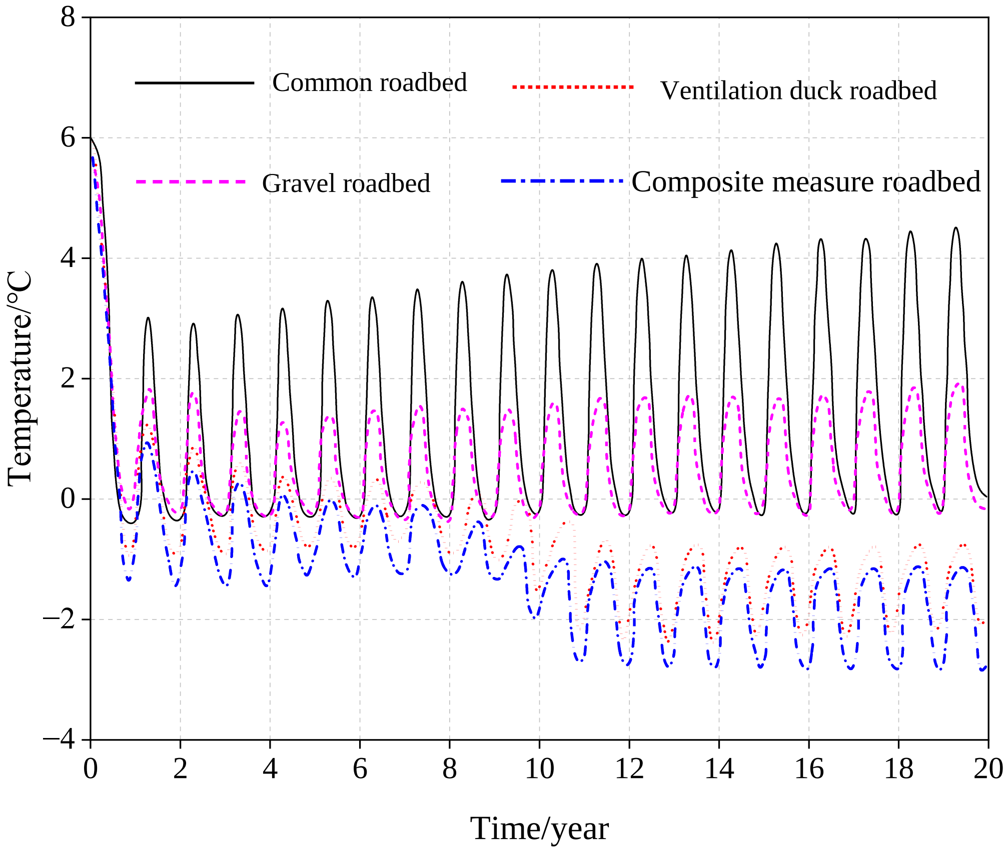

Figure 12. Temperature change at the center of the road base (Point M) after 20 years of operation.

5. Conclusions

1. In the alpine permafrost mountainous area of the Nalati Baluntai section in Xinjiang, the construction of a wide asphalt expressway changed the original ecological balance of the frozen soil. The calculation results show that the maximum melting depth of the left shoulder is 9 m, the maximum melting depth of the subgrade center is 12 m, and the uneven horizontal distribution of the temperature field becomes obvious after 20 years of operation of the half-cut and half-fill subgrade.
2. After 20 years of operation, the maximum thaw depth of the gravel layer roadbed at the centre of the roadbed is 3.85 m, and the maximum thaw depth of the left and right shoulders is 2.95 m; the maximum temperature difference between the original upper permafrost depth and the normal roadbed is approximately 2 °C. After 20 years of

operation, the maximum melt depth at the center at the roadbed is 1.45 m, with a melt rate of 0.18 m/a within the first 12 years; then, it stabilises and the overall temperature below 0 °C at a depth of 3 m below the roadbed after 10 years of operation.

3. After 20 years of operation of the composite gravel layer, the temperature at a depth of 4 m of the subgrade is −2.2 °C, and a frozen area is formed along the slope direction and transverse direction of the subgrade. At this time, the maximum heat absorption at the bottom of the subgrade is 2.1 W/m^2, and the maximum heat release is −2.15 W/m^2. The overall heat absorption and release are basically the same, and the thermal stability of the subgrade is stable.

Author Contributions: Writing—original draft preparation, data curation, Z.C.; funding acquisition, Z.Z.; Supervision, G.L.; Validation, Y.W. All authors have read and agreed to the published version of the manuscript.

Funding: This research was funded by [The Natural Science Foundation of Xinjiang Uygur Autonomous Region] grant number [No. 2020D01C025].

Institutional Review Board Statement: Not applicable.

Informed Consent Statement: Not applicable.

Data Availability Statement: The data used to support the findings of this study are included within the article.

Acknowledgments: The research described in this paper was financially supported by the Natural Science Foundation of Xinjiang Uygur Autonomous Region, No. 2020D01C025.

Conflicts of Interest: The authors declare no conflict of interest.

References

1. Hu, L.Q.; Wu, P.F.; Liang, F.C.; Zhang, W.H. Analyzing the effect of snow cover in spring and winter and air temperature on frozen ground depth in Xinjiang. *J. Glaciol. Geocryol.* **2014**, *36*, 48–54.
2. Yu, Q.; You, Y.; Yan, H.; Liu, X. Distribution and Characteristics of Permafrost in Nalati Mountain, Western Tianshan Mountians in China. *J. Glaciol. Geocryol.* **2013**, *35*, 10–18.
3. Luo, X.; Yu, Q.; Ma, Q.; Guo, L. Study on the heat and deformation characteristics of an expressway embankment with shady and sunny slopes in warm and ice-rich permafrost regions. *Transp. Geotech.* **2020**, *24*, 100390. [CrossRef]
4. Qian, J.; Yu, Q.H.; Gu, W.; You, Y.H. Experimental study of relation between convection process and temperature characteristics of block-stone layer. *Rock Soil Mech.* **2012**, *33*, 83–88.
5. Yu, W.B.; Lai, Y.M.; Zhang, X.F.; Xiao, J.Z. Laboratory experiment study on the ballast and ventilated railway embankment in permafrost regions. *Chin. J. Geotech. Eng.* **2003**, *25*, 436–440.
6. Sun, Z.Z.; Ma, W.; Li, D.Q. Experimental Study on Cooling Effect of Air Convection Embankment with Crushed Rock Slope Protection in Permafrost Regions. *J. Glaciol. Geocryol.* **2004**, *26*, 435–439.
7. Li, S.; Zhang, M.; Pei, W.; Lai, Y.; Yu, W. Thermo-seismic characteristics of a crushed-rock interlayer embankment on a permafrost slope. *COLD Reg. Sci. Technol.* **2018**, *151*, 249–259. [CrossRef]
8. Pei, W.; Zhang, M.; Li, S.; Lai, Y.; Jin, L. Thermo-mechanical stability analysis of cooling embankment with crushed-rock interlayer on a sloping ground in permafrost regions. *Appl. Therm. Eng.* **2017**, *125*, 1200–1208. [CrossRef]
9. Yu, W.B.; Lai, Y.M.; Zhang, X.F.; Xiao, J.Z.; Niu, F.J.; Zhang, S.J. Experimental Study on the Cooling Effect of Block Stone and Crushed Stone. *J. Glaciol. Geocryol.* **2003**, *25*, 638–643.
10. Cheng, G.D.; Sun, Z.Z.; Niu, F.J. Application of Roadbed Cooling Methods in the Qinghai-Tibet Railway Construction. *J. Glaciol. Geocryol.* **2006**, *28*, 797–808.
11. Cheng, G.; Sun, Z.; Niu, F. Application of the roadbed cooling approach in Qinghai-Tibet railway engineering. *Cold Reg. Sci. Technol.* **2008**, *53*, 241–258. [CrossRef]
12. Sun, B.; Yang, L.; Liu, Q.; Wang, W.; Xu, X. Experimental study on cooling enhancement of crushed rock layer with perforated ventilation pipe under air-tight top surface. *Cold Reg. Sci. Technol.* **2011**, *68*, 150–161. [CrossRef]
13. Yu, W.B.; Lai, Y.M.; Niu, F.J.; Zhang, X. Laboratory experiment study on the railway ventilated embankment in permafrost regions. *J. China Railw. Soc.* **2002**, *24*, 78–83.
14. Yu, W.; Lai, Y.; Niu, F.; Zhang, X.F.; Zhang, S.J. Temperature Field Features in the Laboratory Experiment of the Ventilated Railway Embankment in Permafrost Regions. *J. Glaciol. Geocryol.* **2002**, *24*, 601–607.
15. Niu, F.J.; Yu, Q.H.; Lai, Y.M. Analysis of Ground Temperature Change and Thermal Process in the Testing Duct-ventilated Embankment of the Qinghai-Tibet Railway. *J. Glaciol. Geocryol.* **2003**, *25*, 614–620.

16. Niu, F.J.; Cheng, G.D.; Li, J.J.; Ma, W. Experimental Study on the Thermal Boundary Conditions and Temperature Fields of Duct-ventilated Embankment in Permafrost Regions. *J. Glaciol. Geocryol.* **2006**, *28*, 380–389.
17. Yu, Q.; Cheng, G.; Niu, F. Effect Analysis of Auto-Temperature-Controlled Ventilation Roadbed. *Chin. J. Rock Mech. Eng.* **2004**, *23*, 4221–4228.
18. Sun, H.; Ge, X.R.; Zhang, J.Z.; Niu, F.J. Temperature Adjustment Mechanism of Ventilation Pipeline Embankment. *J. Highw. Transp. Res. Dev.* **2013**, *30*, 19–23,37.
19. Song, Z.; Mu, Y.; Ma, W.; Yu, Q.; Xie, S.; Liu, Y. Characteristics and influence factors of wind speed in ventilation duct of ventilation duct embankment in high altitude permafrost regions. *J. Glaciol. Geocryol.* **2021**, *43*, 1111–1120.
20. Sun, H.; Ge, X.; Zhu, D.; Niu, F.; Chen, J. Numerical Investigation of the Temperature Field of a New Convection-Intensifying Composite Embankment in Permafrost Regions. *J. Cold Reg. Eng.* **2019**, *33*, 06018001. [CrossRef]
21. Turner, R. The Foundations of Specification. *J. Log. Comput.* **2005**, *15*, 623–662. [CrossRef]
22. Wang, R.; Liu, Z.; Li, C. Impact of Change in Seasonal Frozen Soil Moisture on Snowmelt Flood in Snowmelt Season. *Res. Soil Water Conserv.* **2013**, *20*, 277–281.
23. Jingzhe, W.; Zhihui, L.; Tiyip, T.; Lan, W.; Bo, Z. Thawing Process of Seasonal Frozen Soil on Northern Slope of the Tianshan Mountains During Snowmelt Period. *Arid Zo. Res.* **2017**, *34*, 282–292.
24. Qin, Z.P.; Lai, Y.M.; Tian, Y.; Zhang, M.Y. Effect of freeze-thaw cycles on soil engineering properties of reservoir bank slopes at the northern foot of Tianshan Mountain. *J. Mt. Sci.* **2021**, *18*, 541–557. [CrossRef]
25. Wang, Q.; Liu, J.; Zhu, X.; Liu, J.; Liu, Z. The experiment study of frost heave characteristics and gray correlation analysis of graded crushed rock. *Cold. Reg. Sci. Technol* **2016**, *126*, 44–50. [CrossRef]
26. Pei, W.; Zhang, M.; Li, S.; Lai, Y.; Jin, L. Enhancement of convective cooling of the porous crushed-rock layer in cold regions based on experimental investigations. *Int. Commun. Heat Mass Transf.* **2017**, *87*, 14–21. [CrossRef]
27. Rui, D.; Zhai, J.; Li, G.; Zhang, J.; Suzuki, T. Field experimental study of the characteristics of heat and water transfer during frost heaving. *Cold Reg. Sci. Technol. 2019 168*, 102892. [CrossRef]
28. Zhang, F.; Guo, L.; Hao, J.; Yang, T. Analyses on the characteristics of seasonally frozen ground under snow cover and forest/grassland in Kunes Valley, western Tianshan, Xinjiang. *J. Glaciol. Geocryol.* **2019**, *41*, 316–323.
29. Liu, M.; Niu, F.; Luo, J.; Yin, G.; Zhang, L. Performance, applicability, and optimization of a new slope cooling and protection structure for road embankment over warm permafrost. *Int. J. Heat Mass Transf.* **2020**, *162*, 120388. [CrossRef]
30. Sun, B.X.; Xu, X.Z.; Lai, Y.M.; Wang, S.J.; Zhang, J.Z. Impact of ballast grain sizes on natural convection cooling effect of embankment in permafrost regions. *Chin. J. Geotech. Eng.* **2004**, *26*, 809–814.
31. Li, Y.; Wang, Q.; Wang, T. Numerical Solution and Test of Results for a Hydrothermal Coupled Model About Frozen Soil. *J. Jilin Univ. Earth Sci. Ed.* **2015**, *45*, 207–213.
32. Ran, H.W.; Fan, J.H.; Huang, J. Review of the coupling of water and heat in the freeze-thaw process and its model of frozen soil. *Pratacultural Sci.* **2019**, *36*, 991–999.
33. Lan, A.; Lin, Z.; Fan, X.; Yao, M. Differences of Surface Energy and Shallow Soil Temperature and Humidity at Sunny and Shady Slopes in Permafrost Region, Beiluhe Basin, Qinghai-Tibet Plateau. *Adv. Earth Sci.* **2021**, *36*, 962–979.
34. Liu, Z.; Yu, X. Coupled thermo-hydro-mechanical model for porous materials under frost action: Theory and implementation. *Acta Geotech.* **2011**, *6*, 51–65. [CrossRef]
35. Qian, J.; Yu, Q.H.; Wu, Q.B.; You, Y.H.; Guo, L. Analysis of asymmetric temperature fields for the duct-ventilated embankment of highway in permafrost regions. *Cold Reg. Sci. Technol.* **2016**, *132*, 1–6. [CrossRef]
36. Li, X.; Yu, Q.; You, Y.; Guo, L. Study of air flow characteristics in ventilation duct of ventilated embankment. *J. Glaciol. Geocryol.* **2016**, *38*, 1300–1307.
37. Liu, M.; Zheng, H.; Niu, F.; Fang, J.; Lin, Z.; Luo, J.; Yin, G. Cooling performance enhancement of a new expressway embankment in the Tibetan Plateau permafrost zone. *COLD Reg. Sci. Technol.* **2021**, *190*, 103345. [CrossRef]
38. Pei, W.; Zhang, M.; Yan, Z.; Li, S.; Lai, Y. Numerical evaluation of the cooling performance of a composite L-shaped two-phase closed thermosyphon (LTPCT) technique in permafrost regions. *Sol. Energy* **2019**, *177*, 22–31. [CrossRef]
39. Zhang, M.; Lai, Y.; Gao, Z.; Yu, W. Influence of boundary conditions on the cooling effect of crushed-rock embankment in permafrost regions of Qinghai-Tibetan Plateau. *Cold Reg. Sci. Technol.* **2006**, *44*, 225–239. [CrossRef]
40. Zhang, M.; Lai, Y.; Li, D.; Tong, G.; Li, J. Numerical analysis for thermal characteristics of cinderblock interlayer embankments in permafrost regions. *Appl. Therm. Eng.* **2012**, *36*, 252–259. [CrossRef]
41. Qin, Y.; Zhang, J. A review on the cooling effect of duct-ventilated embankments in china. *Cold Reg. Sci. Technol.* **2013**, *95*, 1–10. [CrossRef]
42. Zhang, Y.; Haimidan, H.; Gulimire, H.; Liu, Q.; Litan, S. The influence of snowmelt on soil temperature and moisture in different freezingthawing stages on the north slope of Tianshan mountain. *Acta Ecol. Sin.* **2020**, *40*, 1602–1609.
43. Zhu, L.N. Study of the Adherent Layer on Different Types of Ground in Permafrost Regions on the Qinghai-Xizang Plateau. *J. Glaciol. Geocryol.* **1988**, *10*, 8–14.
44. Shi, Y.; Shen, Y.; Hu, R. Preliminary Study on Signal, Impact and Foreground of Climatic Shift from Warm-Dry to Warm-Humid in Northwest China. *J. Glaciol. Geocryol.* **2002**, *24*, 219–226.

45. Zhang, M.; Pei, W.; Zhang, X.; Lu, J. Lateral thermal disturbance of embankments in the permafrost regions of the Qinghai-Tibet Engineering Corridor. *Nat. Hazards* **2015**, *78*, 2121–2142. [CrossRef]
46. Sun, B.X.; Yang, L.J.; Wang, W.; Zhang, J.; Wang, S. Convective heat transfer and evaporative heat removal in embankment with perforated ventilation pipe. *Rock Soil Mech.* **2012**, *33*, 674–680.